JGR Atmospheres

RESEARCH ARTICLE
10.1029/2019JD031011

This article is a companion to Protat et al. (2019) https://doi.org/10.1029/2019JD031010.

Key Points:
- The relationship between radar observables and rainfall properties is different at high latitudes
- There seems to be limited value to the dual-frequency GPM radar measurements for rainfall retrieval
- These results should help improve GPM radar rainfall retrievals

Correspondence to:
A. Protat,
alain.protat@bom.gov.au

Citation:
Protat, A., Klepp, C., Louf, V., Petersen, W. A., Alexander, S. P., Barros, A., et al. (2019). The Llatitudinal Vvariability of oOceanic Rrainfall Pproperties and Iits Iimplication for Ssatellite Rretrievals:. Part 22.: The Relationships Bbetween Radar Observables and Drop Size Distribution Parameters. *Journal of Geophysical Research: Atmospheres*, *124*, 13,312–13,324. https://doi.org/10.1029/2019JD031011

Received 14 MAY 2019
Accepted 16 OCT 2019
Accepted article online 22 OCT 2019
Published online 14 DEC 2019

The Latitudinal Variability of Oceanic Rainfall Properties and Its Implication for Satellite Retrievals: 2. The Relationships Between Radar Observables and Drop Size Distribution Parameters

Alain Protat[1], Christian Klepp[2], Valentin Louf[3], Walter A. Petersen[4], Simon P. Alexander[5], Ana Barros[6], Jussi Leinonen[7], and Gerald G. Mace[8]

[1]Australian Bureau of Meteorology, Melbourne, Victoria, Australia, [2]Land in the Earth System, Max Planck Institute for Meteorology, Hamburg, Germany, [3]School of Earth, Atmosphere and Environment, Monash University, Melbourne, Victoria, Australia, [4]Earth Science Branch, NASA Marshall Space Flight Center, Huntsville, AL, USA, [5]Australian Antarctic Division, Hobart, Tasmania, Australia, [6]Duke University, Durham, NC, USA, [7]École Polytechnique Fédérale de Lausanne, Lausanne, Switzerland, [8]University of Utah, Salt Lake City, UT, USA

Abstract In this study, we develop statistical relationships between radar observables and drop size distribution properties in different latitude bands to inform radar rainfall retrieval techniques and understand underpinning microphysical reasons for differences reported in the literature between satellite mean zonal rainfall products at high latitudes (up to a factor 2 between products over ocean). A major assumption in satellite retrievals is the attenuation-reflectivity relationships for convective and stratiform precipitation. They are found to systematically produce higher attenuation than our relationships with all latitudes included or within individual latitude bands (except in the tropics). The scatter around fitted curves approximating the radar reflectivity-mass-weighted diameter D_m relationship and the dual-frequency ratio (ratio of Ka- to Ku-band reflectivities)-D_m relationships is found to be large and of the same magnitude. This result suggests that the added value of two radar frequencies to improve the D_m retrieval from space seems limited. In contrast, the relationship between D_m and the attenuation/reflectivity ratio is robust and not dependent on latitude. Direct relationships between rainfall and either reflectivity or attenuation are also found to be very robust. Attenuation-reflectivity, D_m-reflectivity, and rainfall rate-reflectivity relationships in the Southern Hemisphere high latitude and Northern Hemisphere polar latitude bands are fundamentally different from those at other latitude bands, producing smaller attenuation, much larger D_m, and lower rainfall rates. This implies that specific relationships need to be used for these latitude bands in radar rainfall retrieval techniques using such relationships.

1. Introduction

The work presented in this paper is the second part of a study aimed at better understanding underpinning microphysical reasons for discrepancies between satellite mean zonal rainfall products at high latitudes in the Northern and Southern Hemispheres reported in the literature (up to a factor 2 between products over the ocean, see Figure 5 in Skofronick-Jackson et al., 2017). As discussed in the first part of this study (Protat et al. 2019, referred to as Part 1 in the following), observing and monitoring global patterns of precipitation and its intensity and detecting long-term changes in precipitation are critically important, and satellites provide an optimal platform from which to measure this. In 2014, the National Aeronautics and Space Administration and the Japan Aerospace Exploration Agency launched the core satellite of the Global Precipitation Measurement (GPM) program, which carries a dual-frequency Ka/Ku precipitation radar (DPR) and a multifrequency passive microwave radiometer for measuring the three-dimensional structure of precipitation globally (Skofronick-Jackson et al., 2017).

GPM is the follow-up mission for the Tropical Rainfall Measurement Mission (TRMM, e.g., Simpson et al., 1988). However, while TRMM focused primarily on the tropical latitudes, GPM with its ~65° inclination enabled analysis of new quantitative radar and microwave radiometer observations of liquid- and mixed-phase precipitation and snow in middle- and high-latitude weather systems (Skofronick-Jackson et al., 2017) not previously sampled by TRMM. GPM precipitation algorithm developers therefore had to adapt

existing tropical rainfall retrieval techniques to convert active and passive measurements from the GPM core observatory into rainfall rates in weather systems that are very different from what was emphasized in the TRMM era from which many of these algorithms were first conceived (Kummerow et al., 2015).

In Part 1, we used a new in situ shipboard global ocean precipitation database produced by the Ocean Rainfall And Ice-phase precipitation measurement Network (OceanRAIN; Klepp et al., 2018) to characterize the natural, latitudinal, and convective-stratiform variability of the drop size distribution (DSD) and compare with current assumptions in GPM radar rainfall retrievals. It has been clearly demonstrated that several assumptions on rainfall microphysics in current GPM algorithms still reflect the TRMM legacy and needed to be revisited. In short, the Southern Hemisphere high latitude (−67.5 °S to −45 °S) and Northern Hemisphere polar latitude (67.5 °N to 90 °N) bands, where mean annual zonal satellite rainfall products most disagree (Grecu et al., 2016; Skofronick-Jackson et al., 2017), were clearly identified as the two regions standing out from the other latitude bands in terms of DSD and associated rainfall properties, with (i) a substantially lower concentration of drops with diameter smaller than 3 mm, (ii) a systematically higher (lower) frequency of occurrence of rainfall rates below (above) 1 mmh^{-1}, (iii) very different values of the DSD shape parameter (μ_0) from what is currently assumed in satellite radar rainfall algorithms, and (iv) very different DSD properties in both the convective and stratiform rainfall regimes, highlighting that both rainfall regimes need attention in satellite retrievals.

Following the work presented in Part 1, the objective of Part 2 (this paper) is to further investigate how these substantial differences in rainfall microphysics translate into differences in statistical relationships between these DSD properties and radar observables, which are the fundamental elements of satellite radar rainfall retrieval techniques. The data sets and methods, which have been described in detail in Part 1, are only briefly recalled in section 2. Relationships between radar observables, DSD parameters, and rainfall rate and their latitudinal variability are derived and analyzed in detail in section 3. Finally, section 4 discusses the main findings of this work.

2. Data Sets and Methods

In this study, DSD properties and radar observables available from satellite platforms are derived from the OceanRAIN database (Klepp et al., 2018), which is a unique in situ global ocean shipboard data set comprising 75 meteorological and oceanographic parameters including precipitation, evaporation, resulting freshwater flux, and surface turbulent fluxes. The precipitation parameters include rain, snow, and mixed-phase precipitation occurrence, intensity, and accumulation, all derived from particle size distribution measurements based on automated ODM470 optical disdrometers. Precipitation rates as low as 0.01 $mm.h^{-1}$ are measured accurately. The OceanRAIN rainfall data set includes the type of rainfall (convective vs stratiform), the main characteristics of the DSD (described below and in more detail in Part 1), and radar reflectivity and attenuation at important frequencies for radar rainfall studies using T-matrix calculations. In total, 126,533 DSD measurements in the OceanRAIN database are available for our analysis. OceanRAIN data are publicly available through the website http://www.oceanrain.org/ and the World Data Center for Climate (data referenced as Klepp et al., 2017).

In order to estimate integral properties of the DSD in Part 1 and investigate the relationship between radar observables and DSD properties in the present study, the DSD is approximated by a normalized gamma distribution (following Testud et al., 2001; Illingworth & Blackman, 2002; and Bringi et al., 2002):

$$N(D) = N_0^* \frac{\Gamma(4)\ (3.67+\mu_0)^{4+\mu 0}}{3.67^4\ \ \Gamma(4+\mu_0)} \left(\frac{D}{D_0}\right)^{\mu_0} exp\left[-(3.67+\mu_0)\frac{D}{D_0}\right]. \quad (1)$$

Using this approximation, the DSD can be characterized with three parameters: N_o^*, the intercept of the distribution; μ_0, the so-called shape parameter of the distribution; and D_0, the median volume diameter of the distribution or D_m, the mass-weighted mean diameter (with $D_0/D_m = (3.67+\mu_0)/(4+\mu_0)$).

To examine statistical relationships between radar observables and DSD properties, radar reflectivity Z_H, and specific attenuation ATT_H, at Ku band (13.6 GHz) and Ka band (35 GHz), which are the two frequencies of the GPM DPR, were estimated from all OceanRAIN DSD measurements using the PyTMatrix code

Table 1
Definition of Latitude Bands and How They Are Referred to in This Study

Latitude band	S-highlat [−67.5; −45]	S-midlat [−45; −22.5]	S-tropics [−22.5; −0]	N-tropics [0; 22.5]	N-midlat [22.5; 45]	N-highlat [45; 67.5]	N-polar [67.5; 90]
Color code	Dark blue	Orange	Red	Red	Orange	Dark blue	Light blue
Line type	Dotted line	Dotted line	Dotted line	Solid line	Solid line	Solid line	Solid line

Note. Color codes and line types for each latitude band are also indicated.

developed by Leinonen (2014). The main assumptions of these T-matrix calculations are the drop shape model and the standard deviation of the drop canting angle (i.e., the angle between the major oblate drop axis and the horizontal axis). In this study, the drop shape model from Thurai et al. (2007) and a standard deviation of the drop canting angle of 10° are used (settings recommended in PyTMatrix).

Finally, in order to characterize the latitudinal variability of relationships between DSD properties and radar observables, we have used the latitude bands, terminology, and color codes described in Table 1. Note that, as explained in Part 1, the southern polar latitude band is not included in our analysis due to an insufficient number of samples in the OceanRAIN database. Sample sizes, limitations, and merits of such latitude band definitions are all discussed in Part 1.

3. Relationships Between Radar Observables, DSD Parameters, and Rainfall Rate and Their Latitudinal Variability

In this section we delve into what can be learned from the OceanRAIN data set in terms of relationships between radar observables currently available from satellite platforms and DSD parameters, how these relationships compare with current GPM radar rainfall algorithm assumptions, how strong the latitudinal variability of these relationships is, and whether this latitudinal variability needs to be included in GPM radar rainfall algorithms.

3.1. Attenuation: Reflectivity Relationships

The two radar observables available from the GPM DPR are the radar reflectivity at Ku (13.8 GHz) and Ka (35 GHz) bands, namely Z_{Ku} and Z_{Ka}. The dual-frequency ratio, $DFR = Z_{Ka}$-Z_{Ku} (dBZ), is also used in DSD parameter retrievals to constrain D_m (Iguchi et al., 2017; Seto et al., 2013; Williams et al., 2014). Power-law relationships between reflectivity and attenuation at the 13.8 GHz and 35 GHz frequencies are also used in GPM radar rainfall algorithms to correct for attenuation. Taking the difference between GPM measurements of the surface backscatter cross section with and without precipitation also provides path-integrated retrieval constraints on attenuation (the so-called surface reference technique). In other words, although not measured directly, Ku-band and Ka-band attenuation (hereafter referred to as ATT_{Ku} and ATT_{Ka}, respectively) and their relationships with Z_{Ku} and Z_{Ka} are used in retrieval algorithms of the DSD parameters. It is therefore worth exploring what the latitudinal variability of such relationships is and how they feed back into variability between these radar observables and DSD parameters. The GPM Version 4 (V04) algorithm was using one reflectivity-attenuation relationship for the convective regime and one for stratiform regime for all latitudes. GPM Version 5 (V05) algorithms introduced an attenuation adjustment factor ε_{Ku} applied to the initial GPM V04 reflectivity-attenuation relationships to account for the global (including latitudinal) variability of the reflectivity-attenuation relationship (Iguchi et al., 2017; Kozu et al., 2009; Seto et al., 2013) as follows:

$$ATT_{Ku} = \varepsilon_{Ku}\,\alpha_{Ku}\;\; Z_{Ku}{}^{\beta_{Ku}}, \tag{2}$$

$$ATT_{Ka} = \varepsilon_{Ka}\,\alpha_{Ka}\;\; Z_{Ka}{}^{\beta_{Ka}}, \tag{3}$$

where (α_{Ku}, β_{Ku}) is 0.0003111 and 0.78069 for stratiform and (α_{Ku}, β_{Ku}) is 0.00042864 and 0.75889 for convective precipitation in GPM retrieval algorithms (Seto et al., 2013). As far as we know, in the current version of the GPM DPR algorithm, $\alpha_{Ka} = 10\,\alpha_{Ku}$ and $\beta_{Ka} = \beta_{Ku}$ (Seto et al., 2013), and the same ε_{Ku} adjustment is applied to attenuation at both radar frequencies (i.e., $\varepsilon_{Ku} = \varepsilon_{Ka}$). The ε_{Ku} correction is derived from

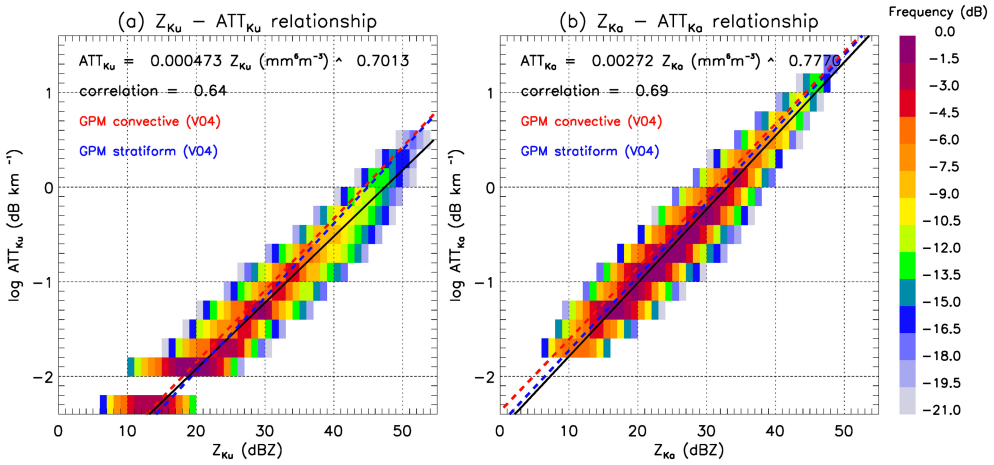

Figure 1. Joint (a) Z_{Ku}-ATT_{Ku} and (b) Z_{Ka}-ATT_{Ka} distributions and associated power-law fits (solid black line). Colors show the number of samples in each bin using a logarithmic scale, defined such that the bin with most occurrences has 0 dB and each 50% decrease in occurrence has a 3-dB decrease on the color scale. The dashed red and blue lines are the GPM V04 convective and stratiform relationships.

independent dual-frequency attenuation retrievals as 5 °× 5° global maps for each precipitation type (convective or stratiform), for each land surface type (land, ocean, and all), and for each month (Iguchi et al., 2017). This attenuation correction adjustment technique was also used in the TRMM algorithms (Iguchi et al., 2000) and was referred to as the "alpha adjustment method." It is important to note that this ε_{Ku} adjustment is also applied in a consistent way to the relationship between rainfall rate and D_m (Iguchi et al., 2017), as was described in Part 1. In Part 1, this rainfall rate-D_m relationship was found to be very different in different latitude bands, fully justifying the use of such ε_{Ku} adjustment technique in GPM algorithms.

Figures 1a and 1b show the attenuation-reflectivity relationship obtained using all points at all latitudes from the OceanRAIN database at Ku and Ka band, respectively. The latitudinal variability of these relationships is shown in Figures 2ac and 2bd for Ku and Ka band, respectively. The corresponding values of the Ku-band and Ka-band power-law fits are also reported in Tables 2 and 3. The correlation between these two radar parameters is slightly higher at Ka band than at Ku band (0.69 vs 0.64), and the relationships are both well approximated by a power law. Our relationship including all latitudes clearly produces systematically smaller attenuation at any given reflectivity than the GPM convective and stratiform relationships, especially at Ku band. The GPM V04 relationships also produce higher attenuation at any given than all individual relationships derived within each latitude band (Figure 2ab). This is further quantified using fractional differences with respect to the general relationship with all latitudes included in Figures 2c and 2d for Ku and Ka band, respectively. From these figures, it is found that for Ku-band reflectivities of 30, 40, and 50 dBZ, the a priori GPM V04 convective relationship produces attenuations 35%, 55%, and 75% higher than

Table 2
Coefficients (e_m, f_m) of the $ATT_{Ku} = e_m Z_{Ku}^{f_m}$ Relationship and Values of the Mean and Standard Deviation of the ε_{Ku} Adjustment for Each Latitude Band as Derived From Figure 12, With ATT_{Ku} in dB km^{-1} and Z_{Ku} in mm^6 m^{-3}

Latitude	S-highlat [−67.5; −45]	S-midlat [−45; −22.5]	S-tropics [−22.5; −0]	N-tropics [0; 22.5]	N-midlat [22.5; 45]	N-highlat [45; 67.5]	N-polar [67.5; 90]
e_m (x10^{-4})	5.222	5.542	4.185	4.728	4.666	5.403	7.531
f_m (x10^{-3})	0.669	0.689	0.734	0.725	0.709	0.686	0.587
Mean (ε_{Ku})	0.83	1.03	1.03	1.11	0.99	0.96	0.64
Std (ε_{Ku})	0.16	0.17	0.15	0.17	0.13	0.17	0.23

Note. The (e_m, f_m) coefficients for the GPM a priori relationships are (3.111 10^{-4}, 0.78069) for stratiform and (4.2864 10^{-4}, 0.75889) for convective rainfall (Seto et al., 2013).

Table 3
Coefficients (g_m, h_m) of the $ATT_{Ka} = g_m Z_{Ka}^{h_m}$ Relationship, With ATT_{Ka} in dB km^{-1} and Z_{Ka} in mm^6 m^{-3}

Latitude	S-highlat [−67.5; −45]	S-midlat [−45; −22.5]	S-tropics [−22.5; −0]	N-tropics [0; 22.5]	N-midlat [22.5; 45]	N-highlat [45; 67.5]	N-polar [67.5; 90]
g_m (x10^{-3})	3.022	3.218	2.756	3.102	2.727	2.984	3.624
h_m (x10^{-3})	0.742	0.762	0.790	0.778	0.782	0.770	0.694

our general relationship including all latitudes. This overestimation is not as large as Ka band: For Ka-band reflectivities increasing from 20 to 50 dBZ, the GPM V04 convective relationship produces attenuations from 45% down to 30% higher than our relationship.

At Ku band, the tropical attenuation-reflectivity relationships produce higher attenuation than the relationship with all latitudes included (by 20% to 35% for reflectivities greater than 30 dBZ, Figure 2c), while again

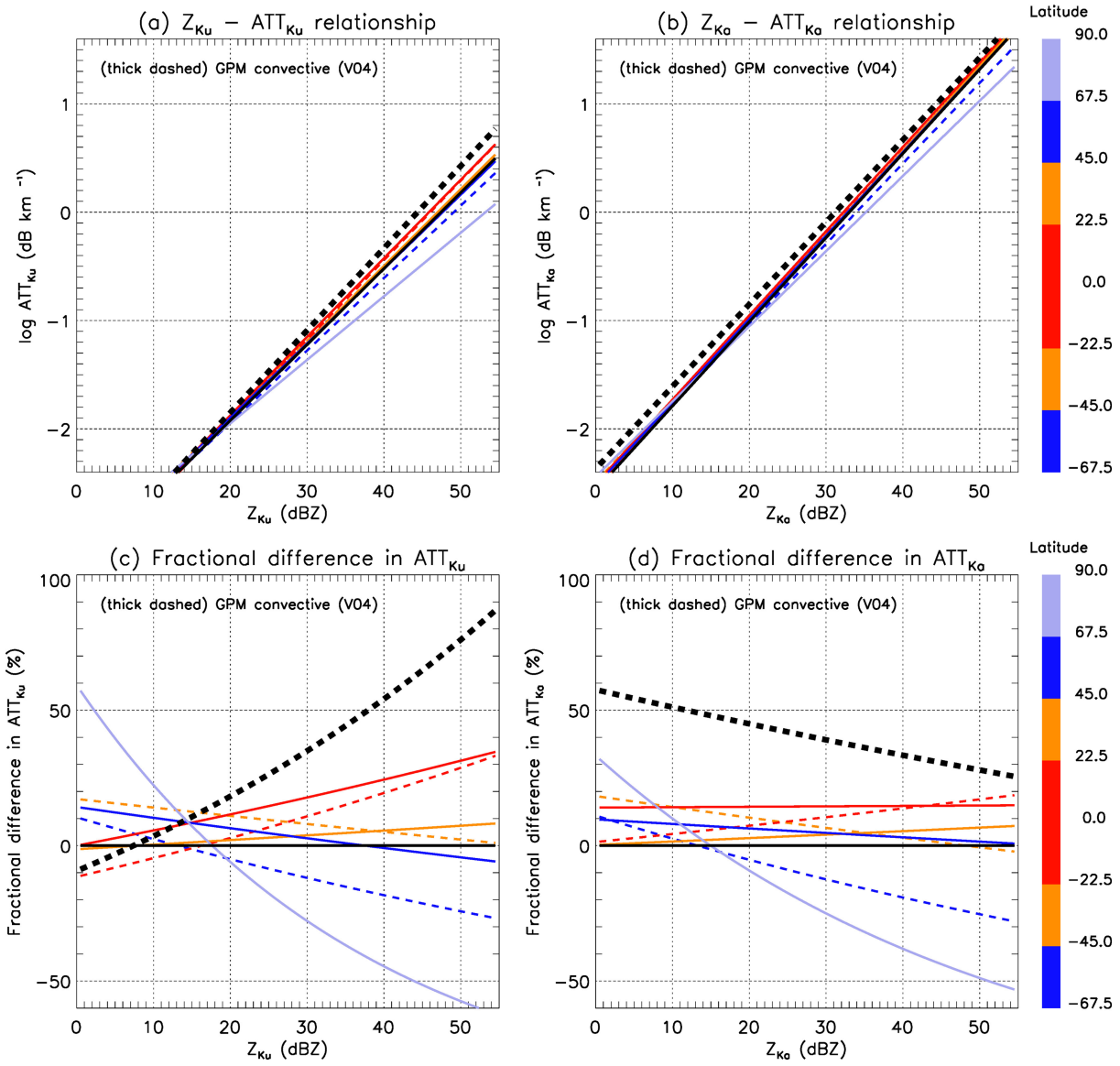

Figure 2. The latitudinal variability of the (a) Z_{Ku}-ATT_{Ku} and (b) Z_{Ka}- ATT_{Ka} relationships and of the (c) fractional differences in (c) ATT_{Ku} as a function of Z_{Ku} and (d) ATT_{Ka} as a function of Z_{Ka} with respect to the general relationship with all latitudes included. The solid black line is our relationship with all latitudes included. Colored lines are for each latitude band (see color bar on the right), with solid lines for the Northern Hemisphere and dashed lines for the Southern Hemisphere. The thicker dashed black line is the GPM V04 convective relationship.

the S-highlat and N-polar bands stand out on these plots as the latitude bands characterized by the lowest attenuation for any given reflectivity above 20 dBZ, where attenuation becomes significant. As an illustration, for a reflectivity of 50 dBZ, attenuation is about 25% lower in the S-highlat band and 50–60% lower in the N-polar band than when using our general relationship (Figure 2cd). Using the a priori GPM V04 relationship would produce extreme overestimations of attenuation in those high-latitude bands (compare thick dashed line with dashed blue and light blue lines in Figure 2cd). The legacy of TRMM algorithm assumptions is again seen in Figure 2a, with our tropical relationships being closest to the assumed GPM V04 relationships.

These lower attenuations as a function of reflectivity in the S-highlat and N-polar bands are consistent with these latitude bands being characterized by much lower drop concentrations N_o^* in Part 1. Attenuation is a lower moment of the DSD than reflectivity, which implies that it is more sensitive to drop concentration than drop diameter. As a result, regions with lower drop concentrations should produce less attenuation for the same reflectivity, which is what is observed in Figure 2cd. In terms of microphysical processes, these lower drop concentrations are linked to much lower cloud condensation nuclei and ice-nucleating particle concentrations observed within pristine high-latitude air masses (e.g., McCluskey et al., 2018).

The TRMM and GPM rainfall retrieval algorithms heavily rely on the accuracy of attenuation estimation (e.g., Iguchi et al., 2000; Iguchi et al., 2017; Meneghini et al., 2000; Seto et al., 2013). It is therefore expected that not accounting for the large latitudinal variability reported in Figure 2 is a significant source of error in the GPM V04 algorithms, where this relationship was held constant globally. It is not straightforward to assess whether the ε_{Ku} adjustments introduced in GPM V05 algorithms capture our estimated latitudinal variability as these adjustments are global maps for each precipitation type, surface type, and month, and they are not yet released as official products. As the GPM algorithms assume that ε_{Ku} follows a log-normal distribution and estimate the mean and standard deviation of this distribution for every retrieval, we show in Figure 3 the full ε_{Ku} distribution derived from our reflectivity-attenuation relationship, as well as the mean and standard deviation of ε_{Ku} for each latitude band (values also reported in Table 2). Our hope is that such information will inform further refinements to the GPM reflectivity-attenuation assumptions. As can be clearly seen from Figure 3, the mean values of ε_{Ku} are close to 1 within each latitude band except the S-highlat and N-polar latitude bands, where the mean values are 0.83 and 0.64, respectively. This result is consistent with the previously discussed results in Figure 2 that these two latitude bands are characterized by lower attenuation at all reflectivities. The main difference between the N-highlat and S-highlat bands is a wider distribution of ε_{Ku} in the N-highlat band with a higher frequency of ε_{Ku} values around 1.5–2.0. The standard deviation of ε_{Ku} is 0.13–0.17 within most latitude bands, but higher (0.23) in the N-polar latitude band. This higher standard deviation in the N-polar band could be partly due to the lower number of samples available in that latitude band to characterize the statistical properties of ε_{Ku}.

3.2. Relationships Between D_m and Radar Observables

As part of the single-frequency and dual-frequency satellite rainfall retrieval processes, a major step is to estimate the mean volume diameter D_m as a function of the observed radar parameters. In single-frequency radar retrievals, a relationship between N_o^* and D_m needs to be assumed to reduce the dimensionality of the retrieval problem down to the number of radar observables (1). D_m is then either retrieved from reflectivity or from the ratio between attenuation and reflectivity (e.g., Seto et al., 2013). In dual-frequency radar retrievals, N_o^* and D_m can be retrieved without needing to assume a relationship between N_o^* and D_m. D_m is first retrieved from the dual-frequency ratio (DFR), and then N_o^* is retrieved from D_m and Z_{Ku} or Z_{Ka}. In this section, we develop such relationships from our OceanRAIN database and investigate their latitudinal variability.

Figure 4 shows the relationship between D_m and reflectivity at Ku or Ka band and the "normalized" relationship between D_m and the ratio (Z/N_o^*). The rationale for normalizing reflectivity by N_o^* is that D_m is the ratio of two moments of the DSD, so it does not depend on N_o^*, while reflectivity is proportional to D_m. When normalizing reflectivity by N_o^*, both Dm and (Z/N_o^*) are independent of N_o^*. In other words, the variability of the reflectivity-D_m relationship due to N_o^* is removed, and the remaining variability is due to details of the DSD. Our Z_{Ku}-D_m relationship including all latitudes (Figure 4a) produces lower D_m than the Williams et al. (2014) relationship for reflectivities above 30 dBZ (dashed black line in Figure 4a). This result suggests that the Williams et al. (2014) relationship, which has been derived from data collected exclusively in Huntsville,

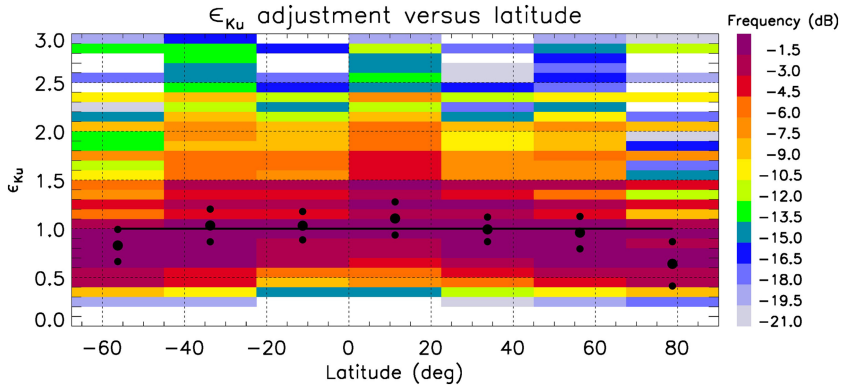

Figure 3. The latitudinal variability of the ε_{Ku} adjustment factor. The ε_{Ku} distribution has been normalized separately for each latitude band. Large black circles are the mean values of ε_{Ku} in each latitude band, and smaller circles are the mean ± standard deviation values of ε_{Ku}. The $\varepsilon_{Ku} = 1.0$ value is drawn as a horizontal black line for reference. Colors show the number of samples in each bin using a logarithmic scale explained in the caption to Figure 1.

Alabama, probably overestimated D_m in other latitude bands. The correlation between D_m and reflectivity is higher at Ku band than at Ka band (0.73 vs 0.68). Overall the scatter of the Z-D_m relationships is found to be quite large. However, when normalizing reflectivity by N_o^* (Figures 4b and 4d), the correlation between D_m and (Z/N_o^*) becomes very high (>0.95). The important implication for radar rainfall retrievals is that if D_m

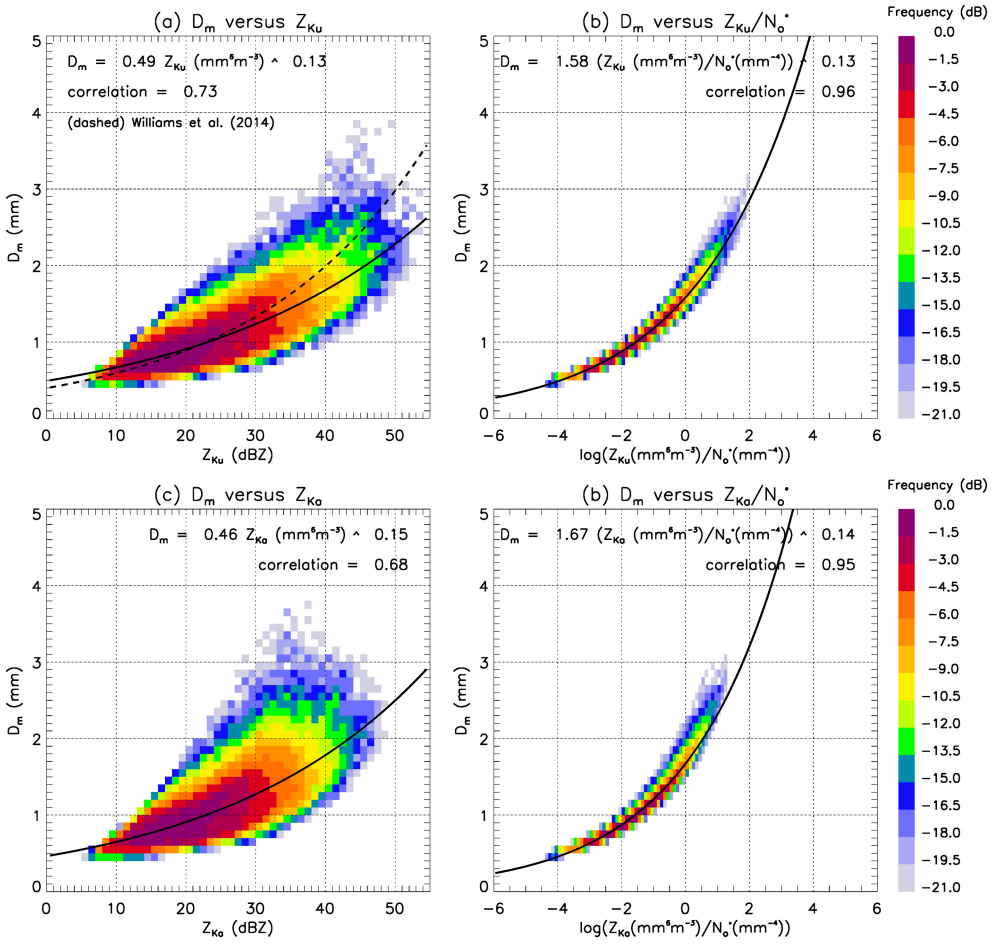

Figure 4. Joint (a) Z_{Ku}-D_m, (b) (Z_{Ku}/N_o^*)-D_m, (c) Z_{Ka}-D_m, and (d) (Z_{Ka}/N_o^*)-D_m distributions and associated power-law fits (solid black lines). The dashed line in panel (a) is the Williams et al. (2014) relationship. Colors show the number of samples in each bin using a logarithmic scale explained in the caption to Figure 1.

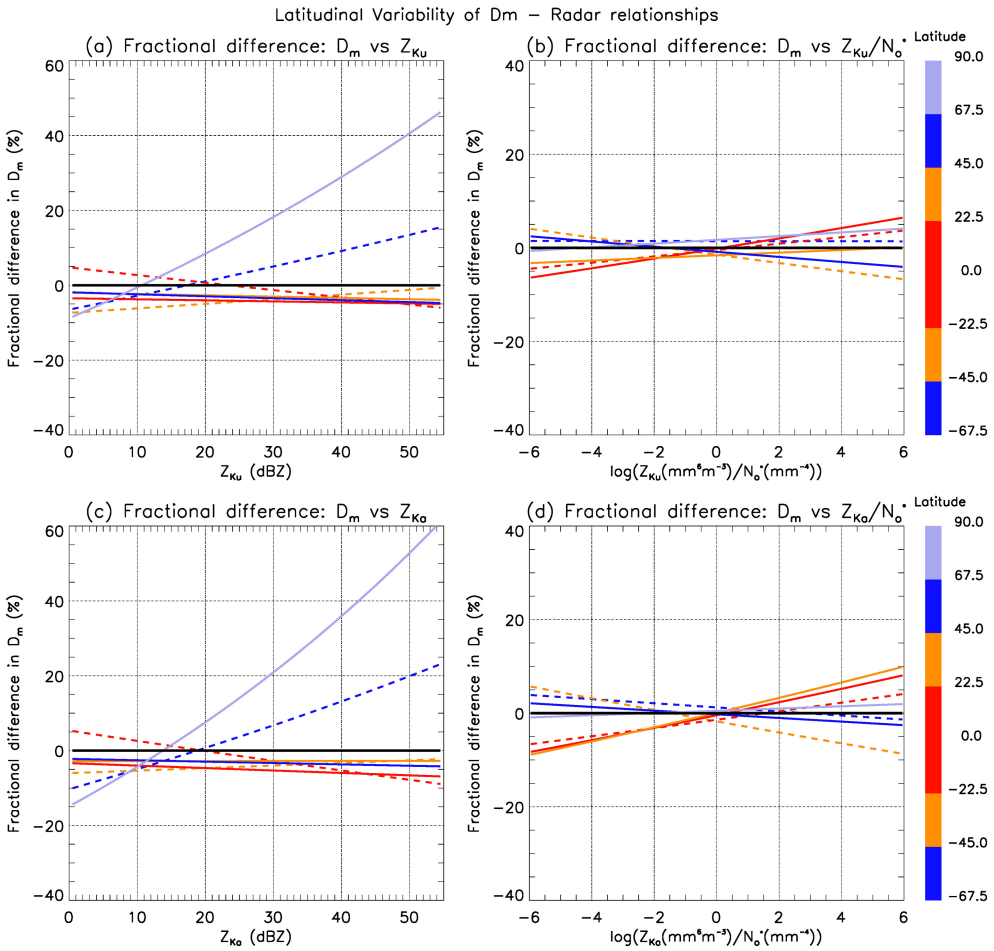

Figure 5. The fractional differences in D_m with respect to the general relationships with all latitudes included using the (a) Z_{Ku}-D_m, (b) (Z_{Ku}/N_o^*)-D_m, (c) Z_{Ka}-D_m, and (d) (Z_{Ka}/N_o^*)-D_m relationships. Colored solid and dotted lines are for each latitude band (see color bar on the right). Solid (dotted) lines are Northern Hemisphere (Southern Hemisphere) results from each latitude band.

can be retrieved accurately, then N_o^* can also be retrieved accurately from Z and D_m using our proposed normalized relationships. This high correlation between D_m and (Z/N_o^*) also shows that the large scatter of the Z-D_m relationships is most exclusively due to the large variability of N_o^* documented in Part 1.

The latitudinal variability of these Z-D_m and (Z/N_o^*)-D_m relationships is explored in Figure 5 using fractional differences with respect to the "general" relationship (i.e., the relationship obtained when including all latitudes). Coefficients of the power-law Z-D_m fits within each latitude band are also given in Tables 4 and 5 at Ku and Ka band, respectively. As has been found for several other relationships in this study, the S-highlat and N-polar bands stand out as being characterized by substantially different Z-D_m relationships (Figure 5ac), with up to 20–25% higher D_m in the S-highlat band and up to 60% higher D_m in the N-polar band for the highest reflectivities. This large variability suggests that radar rainfall algorithms making use of such

Table 4
Coefficients (i_m, j_m) of the $D_m = i_m Z_{Ku}^{j_m}$ Relationship for Each Latitude Band, with D_m in mm and Z_{Ku} in $mm^6 m^{-3}$

Latitude	S-highlat [−67.5; −45]	S-midlat [−45; −22.5]	S-tropics [−22.5; −0]	N-tropics [0; 22.5]	N-midlat [22.5; 45]	N-highlat [45; 67.5]	N-polar [67.5; 90]
i_m	0.459	0.455	0.515	0.474	0.482	0.482	0.448
j_m	0.150	0.139	0.125	0.132	0.129	0.131	0.171

Table 5
Coefficients (k_m, l_m) of the $D_m = k_m Z_{Ka}^{l_m}$ Relationship for Each Latitude Band, With D_m in mm and Z_{Ka} in $mm^6\ m^{-3}$

Latitude	S-highlat [−67.5; −45]	S-midlat [−45; −22.5]	S-tropics [−22.5; −0]	N-tropics [0; 22.5]	N-midlat [22.5; 45]	N-highlat [45; 67.5]	N-polar [67.5; 90]
k_m	0.415	0.435	0.488	0.448	0.450	0.453	0.394
l_m	0.172	0.149	0.135	0.143	0.146	0.145	0.197

relationships should include an adjustment for the S-highlat and N-polar bands. The other latitude bands are characterized by very similar relationships to the general one including all latitudes, with fractional differences with the general relationship being less than 10% over the whole reflectivity range (Figure 5). In contrast, the normalized (Z/N_o^*)-D_m relationships at Ku and Ka band do not vary much with latitude (Figure 5bd, less than 10% fractional difference with the general relationship), which suggests again that the large latitudinal variability of the Z-D_m relationships is predominantly due to the large variability of N_o^* with latitude observed in Part 1.

Single-frequency radar GPM algorithms are based on a relationship between D_m and the (ATT_{Ku}/Z_{Ku}) or (ATT_{Ka}/Z_{Ka}) ratio, derived from T-matrix scattering calculations and DSD assumptions discussed in Seto et al. (2013) and Kozu et al. (2009). The D_m-(ATT/Z) relationships at Ku and Ka band are shown in Figure 6. Power-law fits are also proposed in this figure. The correlation between these two variables is high at both frequencies, and highest at Ka band (0.85 vs 0.91), indicating that this relationship is very robust. The latitudinal variability of these relationships is also found to be very small (not shown). The implication of this result is that when attenuation can be accurately estimated from space, D_m should also be accurately retrieved using such D_m-(ATT/Z) relationships.

Dual-frequency GPM rainfall retrievals use a relationship between DFR and D_m (Iguchi et al., 2017; Seto et al., 2013). As observed in Figure 7, there is indeed a well-defined but complex relationship, not fully captured by our third-degree polynomial fit. This complex relationship, as already discussed in Matrosov et al. (2005) and Leinonen et al. (2012), arises from a coincidental positive scattering resonance at the Ka band at diameters ranging from about 0.9 to 2.4 mm, which forces the Ka band reflectivity to be slightly higher than that at the Ku band. The main implication from a D_m retrieval standpoint is that there are two D_m solutions for all positive values of DFR. In the official GPM dual-frequency radar retrieval scheme (Seto et al., 2013), the highest value of D_m is systematically selected. Unfortunately, this DFR-D_m relationship is characterized by a large variability, as indicated by a correlation of −0.72. Using this type of relationship will therefore introduce substantial errors in the dual-frequency retrievals. This correlation is similar to the correlation obtained with Z_{Ku} or Z_{Ka} alone (Figure 4ac), despite the removal of the variability due to N_o^* when calculating the dual-frequency ratio (Iguchi et al., 2017). Further investigations using the latitude bins reveal that the latitudinal

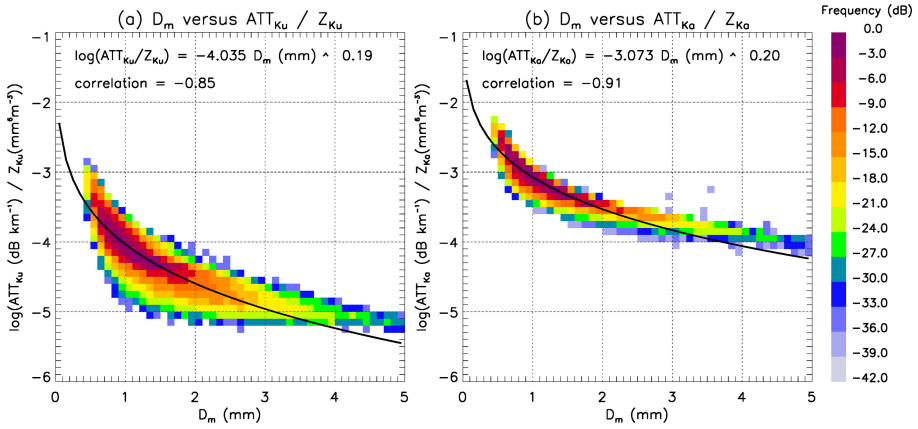

Figure 6. Joint (a) D_m-(ATT_{Ku}/Z_{Ku}) and (b) D_m-(ATT_{Ka}/Z_{Ka}) distributions and associated power-law fits (solid black lines). Colors show the number of samples in each bin using a logarithmic scale explained in the caption to Figure 1.

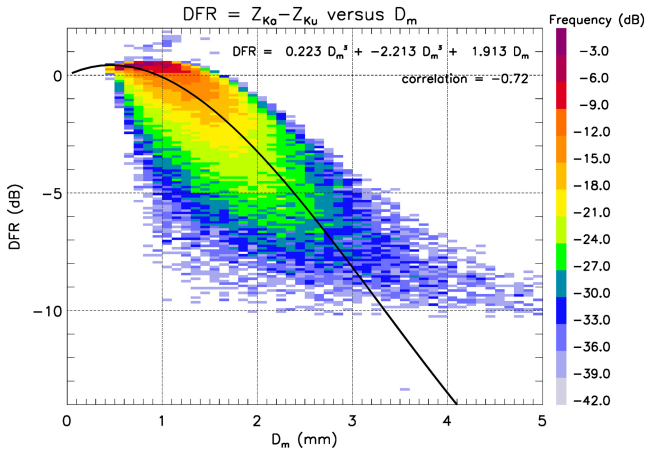

Figure 7. Joint *DFR-D_m* distribution and third-order polynomial fit to the data (solid black line). Colors show the number of samples in each bin using a logarithmic scale explained in the caption to Figure 1.

variability of the *DFR-D_m* relationship is small (not shown) and does unfortunately not explain any of the observed scatter in Figure 7. That leaves the natural variability of the DSD parameters (D_m, μ_0, and the functional form of the DSD) as the most likely source of variability of this relationship. To our knowledge, this large variability of the *DFR-D_m* relationship has only rarely been acknowledged in the literature (Matrosov

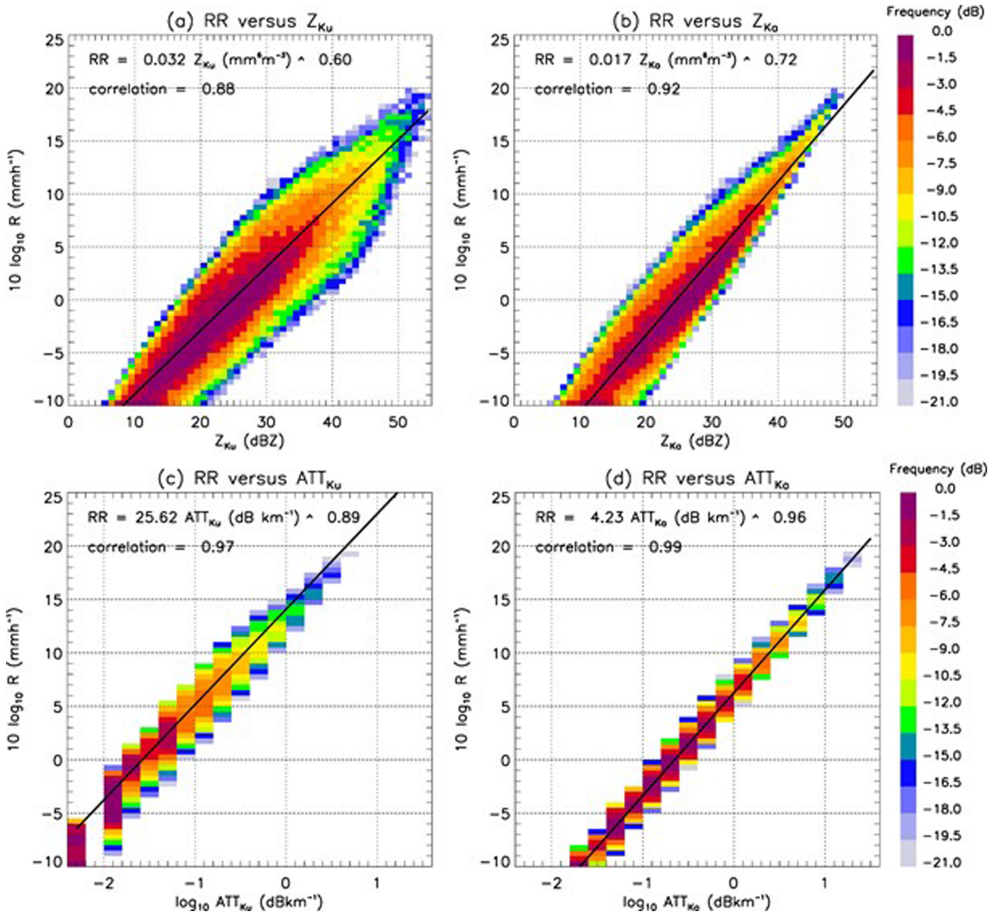

Figure 8. Same as Figure 4 but for the joint (a) Z_{Ku}-R, (b) Z_{Ka}-R, (c) ATT_{Ku}-R, and (d) ATT_{Ka}-R distributions. Colors show the number of samples in each bin using a logarithmic scale explained in the caption to Figure 1.

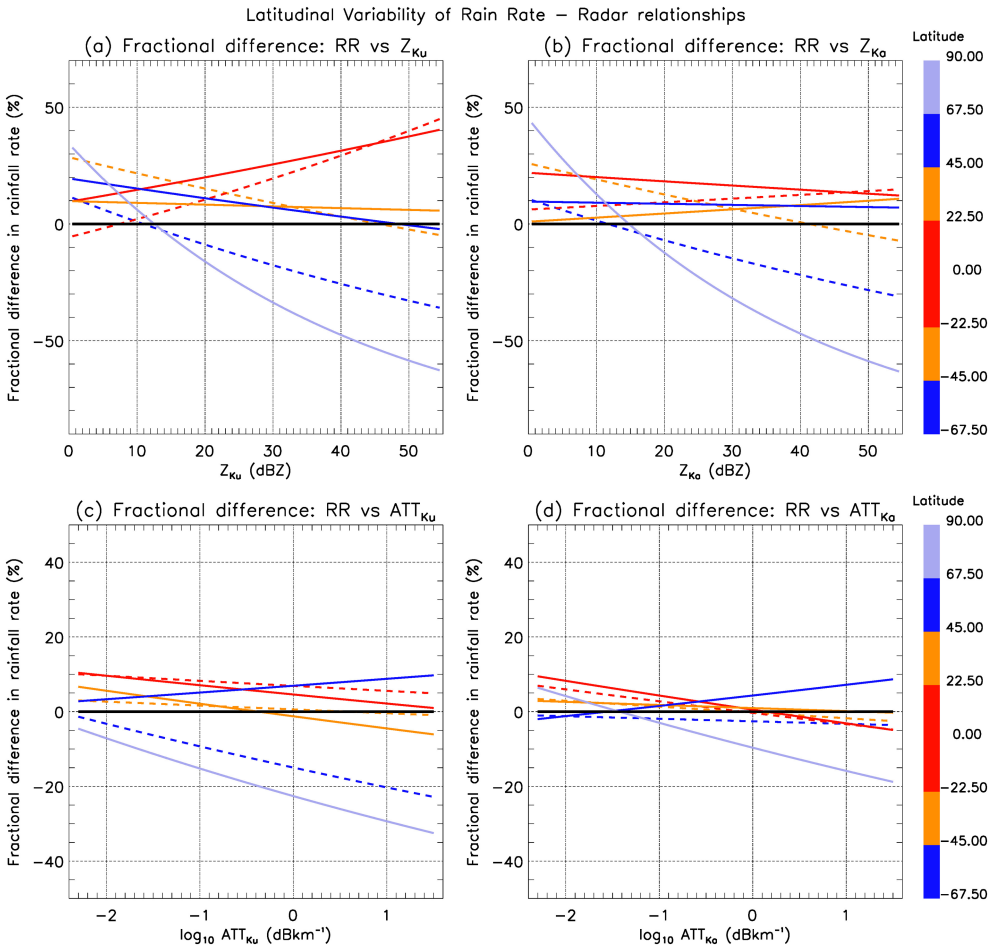

Figure 9. Same as Figure 5 but for the fractional differences in *R* with respect to the general relationships with all latitudes included using the (a) Z_{Ku}-*R*, (b) Z_{Ka}-*R*, (c) ATT_{Ku}-*R*, and (d) ATT_{Ka}-*R* relationships.

et al. 2005; Leinonen et al. 2012). This result may also have implications for the development of new dual-frequency radar rainfall algorithms.

3.3. Relationships Between Rainfall Rate and Radar Observables

In GPM radar algorithms, rainfall rate *R* is derived at the end of the retrieval process from D_m, using empirical relationships for convective and stratiform rainfall regimes (Iguchi et al., 2017, Part 1). Other traditional ways to retrieve rainfall rates from radar observables are to use empirical radar reflectivity-rainfall rate and attenuation-rainfall rate relationships. The OceanRAIN data set provides an opportunity to investigate the accuracy and latitudinal variability of these relationships. Such relationships can also be introduced in satellite radar rainfall retrieval algorithms.

Figure 8 shows the *Z*-*R* and *ATT*-*R* relationships at Ku and Ka band. These relationships are all found to be very robust, with rainfall rate boasting very high correlations of 0.88 and 0.92 with Z_{Ku} and Z_{Ka}, respectively,

Table 6
Coefficients ($\boldsymbol{m_m}$, $\boldsymbol{n_m}$) of the $\boldsymbol{R = m_m Z_{Ku}}^{\boldsymbol{n_m}}$ Relationship for Each Latitude Band, With R in mmh^{-1} and Z_{Ku} in $mm^6\ m^{-3}$

Latitude	S-highlat [−67.5; −45]	S-midlat [−45; −22.5]	S-tropics [−22.5; −0]	N-tropics [0; 22.5]	N-midlat [22.5; 45]	N-highlat [45; 67.5]	N-polar [67.5; 90]
$\boldsymbol{m_m}$	0.0359	0.0413	0.0303	0.0352	0.0353	0.0384	0.0431
$\boldsymbol{n_m}$	0.557	0.578	0.636	0.621	0.598	0.586	0.500

Table 7
Coefficients (o_m, p_m) of the $R = o_m Z_{Ka}^{p_m}$ Relationship for Each Latitude Band, with R in mmh^{-1} and Z_{Ka} in $mm^6 m^{-3}$

Latitude	S-highlat [−67.5; −45]	S-midlat [−45; −22.5]	S-tropics [−22.5; −0]	N-tropics [0; 22.5]	N-midlat [22.5; 45]	N-highlat [45; 67.5]	N-polar [67.5; 90]
o_m	0.0183	0.0209	0.0176	0.0202	0.0167	0.0182	0.0240
p_m	0.687	0.700	0.731	0.718	0.732	0.723	0.615

and 0.97 and 0.99 with ATT_{Ku} and ATT_{Ka}, respectively. It is worth recalling at this stage that these reflectivities and attenuations are not measured quantities but T-matrix estimates using measured DSDs as inputs. In other words, the variability of the relationships between rainfall rate, reflectivity, and attenuation generated by T-matrix calculations only comes from the natural variability of the DSDs, which is important and relevant, but does not include radar noise in the measurements and errors associated with attenuation retrievals. The latitudinal variability of the Z_{Ku}-R (Figure 9a, Table 6) and Z_{Ka}-R (Figure 9b, Table 7) relationships is due to the S-highlat and N-polar bands being characterized by systematically lower rainfall rates (minima of −40% and −60%, respectively) and the tropical bands being characterized by systematically higher rainfall rates (maxima of 40–45%) for the same reflectivity (Figure 9a). In contrast, the latitudinal variability of the Ka-band relationship is mostly due to the lower rainfall rates within the S-highlat and N-polar bands (minima of −30% and −60%, respectively, for the highest reflectivities). Overall the latitudinal variability of the ATT-R relationships is smaller than that of the Z_{Ku}-R relationship at Ku band (minima of −25% and −35%, respectively, for the S-highlat and N-polar bands (Figure 9c), and much smaller at Ka band (less than 20% variability, Figure 9d), which is an interesting feature that could be further exploited in satellite radar rainfall retrievals. As discussed in Part 1, these systematically lower rainfall rates in the S-highlat and N-polar bands are consistent with the lower number concentrations N_o^*, since rainfall rate is proportional to N_o^*, while D_m, being a ratio of the fourth to the third moment of the DSD, does not depend on N_o^*. As discussed previously, these lower drop concentrations are due to much lower cloud condensation and ice nuclei concentrations observed at high latitudes (e.g., McCluskey et al., 2018).

Although a direct link cannot be established, it is important to note that the obtained latitudinal variability in the S-highlat and N-polar bands is of a magnitude similar to that of the reported difference of up to a factor 2 between satellite rainfall zonal-mean rainfall estimates over the ocean at these high latitudes (Skofronick-Jackson et al., 2017). This suggests that these systematic satellite rainfall biases could potentially be mitigated by using tailored relationships proposed in this study. This will be the next step of this work.

4. Summary and Conclusions

The aim of this two-part study was to better understand underpinning microphysical reasons for the large discrepancies between satellite rainfall products at high latitudes in the Northern and Southern Hemispheres reported in the literature. To do so, we have characterized the latitudinal variability of the convective and stratiform DSD properties (Part 1) and developed and analyzed relationships between radar observables and DSD parameters (Part 2, this paper) using a new in situ shipboard global ocean precipitation database produced by the OceanRAIN project (Klepp et al., 2018).

A crucial underlying assumption in GPM radar algorithms is the statistical relationship between attenuation and reflectivity at Ku and Ka band. An important result of our study is that our attenuation-reflectivity relationships produce systematically smaller attenuation at any given reflectivity than the GPM V04 convective and stratiform relationships within all latitude bands (although it is close for the tropical bands), especially at Ku band. This smaller attenuation property is most pronounced within the S-highlat and N-polar bands. We speculate that this could have a major impact on the accuracy of GPM rainfall retrievals at high latitudes. Whether the spatial adjustment (ε_{Ku}) now included in the GPM V05 algorithms has solved this issue could not be readily assessed. Therefore, we have derived from the OceanRAIN data set our own ε_{Ku} latitudinal adjustment (and its standard deviation for probabilistic retrievals) of the attenuation-reflectivity relationships that could be used in GPM radar rainfall retrievals or compared to the current values introduced in GPM V05 algorithms. In terms of the D_m retrieval, the relationships between radar reflectivity (Ku or Ka band) and D_m were found to be quite scattered. The relationships for the S-highlat and N-polar bands are

again very different from those within other latitude bands, which means that specific relationships need to be used for these latitude bands in radar rainfall retrieval schemes using such relationships. Unfortunately, the DFR-D_m relationship is found to be similarly scattered around the fitted curve, suggesting that the added value of having two radar frequencies for the D_m retrieval seems limited. In contrast, the relationship between D_m and the ratio (attenuation/reflectivity) at either Ku or Ka band was found to be very robust (correlations of 0.85 and 0.91, respectively) and not dependent on latitude. Finally, direct relationships between rainfall and either reflectivity or attenuation at Ku and Ka band are found to be very robust. However, we found a noticeable latitudinal variability of the *Z-R* relationships, which is mostly due to the S-highlat and N-polar bands being characterized by substantially lower rainfall rates than in the other latitude bands for the same reflectivity. Again, this result implies that radar retrievals using such *Z-R* relationships need to account for this latitudinal variability.

Our next natural step will be to liaise with GPM algorithm developers and work on introducing the latitudinal variability of statistical rainfall properties where appropriate and then evaluating the resulting statistical improvement in rainfall statistics in the high latitudes using the OceanRAIN database.

Acknowledgments
The sustained funding by Initiative Pro Klima (Mabanaft, Mabanaft Deutschland, Petronord, and OIL! Tankstellen GmbH & Co. KG) enabled the development, operation, and research on OceanRAIN. We greatly appreciate this support and gratefully thank Tanja Thiele, Gerhard Grambow, Volker Tiedemann, Ulrich Freudental, and Jan Falke. The project was hosted and cofunded by CliSAP/CEN, University of Hamburg, and the Max Planck Society (MPG). The authors wish to acknowledge the contribution of the Australian Marine National Facility MNF (Brett Muir and Will Ponsonby) for their help setting up and taking care of the ODM470 disdrometer on RV Investigator and Dr. Toshio Iguchi from the National Institute of Information and Communications Technology, Japan, for useful discussions about details of the GPM dual-frequency radar rainfall algorithm. The Australian Antarctic Division's contribution was supported by project 4387 of the Australian Antarctic program. OceanRAIN data are publicly available through the website http://www.oceanrain.org/ and the World Data Center for Climate (data referenced as Klepp et al. 2017ab).

References

Bringi, V. N., Huang, G., Chandrasekar, V., & Gorgucci, E. (2002). A methodology for estimating the parameters of a gamma raindrop size distribution model from polarimetric radar data: Application to a squall-line event from the TRMM/Brazil Campaign. *J. Atmos. Oceanic Technol.*, *19*, 633–645.

Grecu, M., Olson, W. S., Munchak, S. J., Ringerud, S., Liao, L., Haddad, Z. S., et al. (2016). The GPM combined algorithm. *J. Atmos. Oceanic Technol.*, *33*, 2225–2245. https://doi.org/10.1175/JTECH-D-16-0019.1

Iguchi, T., Kozu, T., Meneghini, R., Awaka, J., & Okamoto, K. (2000). Rain-profiling algorithm for the TRMM precipitation radar. *J. Appl. Meteor.*, *39*, 2038–2052.

Iguchi, T., S. Seto, R. Meneghini, N. Yoshida, J. Awaka, M. Le, et al., 2017: GPM/DPR Level-2 Algorithm Theoretical Basis Document. Available at https://pmm.nasa.gov/sites/default/files/document_files/ATBD_DPR_201708_whole_1.pdf

Illingworth, A. J., & Blackman, T. M. (2002). The need to represent raindrop size spectra as normalized gamma distributions for the interpretation of polarization radar observations. *J. Appl. Meteor.*, *41*, 286–297.

Klepp, C., Michel, S., Protat, A., Burdanowitz, J., Albern, N., Dahl, A., et al. (2018). OceanRAIN, a new in-situ shipboard global ocean surface-reference dataset of all water cycle components. *Nature—Scientific Data*. https://doi.org/10.1038/sdata.2018.122

Klepp, C., Michel, S., Protat, A., Burdanowitz, J., Albern, N., Louf, V., et al. (2017). Ocean Rainfall And Ice-phase precipitation measurement Network - OceanRAIN-M. *World Data Center for Climate (WDCC) at DKRZ*. http://doi.org/10.1594/WDCC/OceanRAIN-M

Kozu, T., Iguchi, T., Shimomai, T., & Kashiwagi, N. (2009). Raindrop size distribution modeling from a statistical rain parameter relation and its application to the TRMM Precipitation Radar rain retrieval algorithm. *J. Appl. Meteor. Climatol.*, *48*, 716–724.

Kummerow, C., Randel, D. L., Kulie, M., Wang, N.-Y., Ferraro, R., Munchak, S. J., & Petkovic, V. (2015). The evolution of the Goddard profiling algorithm to a fully parametric scheme. *J. Atmos. Oceanic Technol.*, *32*, 2265–2280. https://doi.org/10.1175/JTECH-D-15-0039.1

Leinonen, J. (2014). High-level interface to T-matrix scattering calculations: Architecture, capabilities and limitations. *Optics express*, *22*(2), 1655–1660. https://doi.org/10.1364/OE.22.001655

McCluskey, C. S., Hill, T. C. J., Humphries, R. S., Rauker, A.-M., Moreau, S., Strutton, P. G., et al. (2018). Observations of ice nucleating particles over Southern Ocean waters. *Geophys. Res. Letters*, *45*. https://doi.org/10.1029/2018GL079981

Meneghini, R., Iguchi, T., Kozu, T., Liao, L., Okamoto, K., Jones, J., & Kwiatkowski, J. (2000). Use of the surface reference technique for path attenuation estimates from the TRMM precipitation radar. *Journal of Applied Meteorology*, *39*(12), 2053–2070.

Seto, S., Iguchi, T., & Oki, T. (2013). The basic performance of a precipitation retrieval algorithm for the Global Precipitation Measurement mission's single/dual-frequency radar measurements. *IEEE Trans. Geosci. Remote Sens.*, *51*, 5239–5251.

Simpson, J. R., Adler, R. F., & North, G. R. (1988). A proposed Tropical Rainfall Measuring Mission (TRMM) satellite. *Bull. Amer. Meteor. Soc.*, *69*, 278–295.

Skofronick-Jackson, G., Petersen, W. A., Berg, W., Kidd, C., Stocker, E. F., Kirschbaum, D. B., et al. (2017). The Global Precipitation Measurement (GPM) Mission for Science and Society. *Bull. Amer. Meteor. Soc.*, *98*, 1679–1695.

Testud, J., Oury, S., Black, R. A., Amayec, P., & Dou, X. K. (2001). The concept of "normalized" distribution to describe raindrop spectra: A tool for cloud physics and cloud remote sensing. *J. Appl. Meteor.*, *40*, 1118–1140.

Thurai, M., Huang, G. J., Bringi, V. N., Randeu, W. L., & Schönhuber, M. (2007). Drop shapes, model comparisons, and calculations of polarimetric radar parameters in rain. *J. Atmos. Oceanic Technol.*, *24*, 1019–1032.

Williams, C. R., Bringi, V. N., Carey, L. D., Chandrasekar, V., Gatlin, P., Haddad, Z., et al. (2014). Describing the shape of raindrop size distributions using uncorrelated raindrop mass spectrum parameters. *Journal of Applied Meteorology and Climatology*, *53*(5), 1282–1296.